J Solid State Electrochem (2008) 12:879–884
DOI 10.1007/s10008-007-0477-z

ORIGINAL PAPER

Effect of acid treatment of $Co_{rich\ core}$–$Pt_{rich\ shell}$/C electrocatalyst on oxygen reduction reaction

Mei-Hua Lee · Pei-Shan Wang · Jing-Shan Do

Received: 1 July 2007 / Revised: 30 October 2007 / Accepted: 1 November 2007 / Published online: 4 April 2008

Abstract $Co_{rich\ core}$–$Pt_{rich\ shell}$/C prepared by thermal decomposition and chemical reduction methods were treated by 20% H_2SO_4 aqueous solution and used as the electrocatalysts for the oxygen reduction reaction (ORR). The particle size range of $Co_{rich\ core}$–$Pt_{rich\ shell}$ (molar ratio of 0.92:1) on carbon powder support decreased from 3–8 to 1–6 nm when the time for the electrocatalysts immersed and treated with 20% H_2SO_4 aqueous solution increased from 0 to 4 h. Using $Co_{rich\ core}$–$Pt_{rich\ shell}$ (molar ratio of 0.92:1)/C treated with 20% H_2SO_4 from 0 to 4 h as the working electrode, the open circuit potential of ORR in 0.5 M $HClO_4$ aqueous solution increased from 0.9995 to 1.0155 V, and the current density, mass activity, and specific activity at the overpotential of 0.1 V increased from 0.619 mA cm^{-2}, 6.184 A g^{-1}, and 18.614 μA cm^{-2} to 0.912 mA cm^{-2}, 15.544 A g^{-1}, and 23.413 μA cm^{-2}, respectively.

Keywords Fuel cell · $Co_{rich\ core}$–$Pt_{rich\ shell}$ · Oxygen reduction reaction · Acid treatment

Contribution to ICMAT 2007, Symposium K: Nanostructured and bulk materials for electrochemical power sources, July 1–6, 2007, Singapore.

M.-H. Lee · P.-S. Wang · J.-S. Do (✉)
Center of Nanoscience and Nanotechnology and Department of Chemical Engineering, Tunghai University,
40704 Taichung, Taiwan
e-mail: jsdo@thu.edu.tw

M.-H. Lee
Department of Industrial Engineering and Management,
Diwan College of Management,
72141 Madou, Tainan, Taiwan

Introduction

The invention of fuel cell as energy conversion systems dates from the middle of the nineteenth century. In the recent years, the development of fuel cells received more and more attention due to its low emission of pollutants, less corrosion problems, and high energy conversion efficiency. Furthermore, the increase in the importance of fuel cells is due to the shortage in the fossil fuels and the increase in CO_2 emission. The polymeric electrolyte membrane fuel cell (PEMFC), one kind of fuel cells, is an endurable, quite, light, clean, and efficient energy conversion device for transportation application. However, the overall efficiency of PEMFC is generally limited by the oxygen reduction reaction (ORR) on the cathode due to its slow kinetics. Although a variety of metallic catalysts have been investigated, the Pt-based electrocatalysts exhibit a higher activity for ORR [1]. Therefore, electrocatalysts with high utility and low loading of the expensive Pt are developed to make the cost of fuel cells decrease [2]. Furthermore, Pt alloyed with the other transition metals (Pt–M, M=Fe, Co, Cr, V, Mn, etc.) exhibit a higher electrocatalytic activity and also reduce the cost of electrocatalysts and fuel cells [3–6].

The effect of transition metal ions, such as Fe^{3+}, Co^{2+}, Ni^{2+}, and Cu^{2+} added into the electrolyte of fuel cells, on the properties and performances of fuel cells were investigated in the literature [7–11]. The dissolution of Fe, Ni, and Co metals from Pt–Fe, Pt–Ni, and Pt–Co used as the cathodic electrocatalysts results in the decrease of its electrocatalytic activity [12]. One possible way to overcome the dissolution of transition metal from Pt–M is to prepare the transition metals in core and Pt in shell ($M_{rich\ core}$–

$Pt_{rich\ shell}$) type of electrocatalyst. Using $M_{rich\ core}$–$Pt_{rich\ shell}$ as the electrocatalyst of ORR, the transition metal (M) at the core can be protected by the Pt at the shell, and the dissolution of the transition metal and the decay of the electroactivity may be inhibited. The effect of thermal annealing on the properties of $Co_{rich\ core}$–$Pt_{rich\ shell}$/C is studied in our previous study [13]. The $Co_{rich\ core}$–$Pt_{rich\ shell}$/C electrocatalyst annealed in air exhibited the higher mass activity (MA) and specific activity (SA) of ORR, which were 10.07 A g^{-1} and 11.27 μA cm^{-2}, were 2.45- and 1.84-fold of Pt/C annealed in air, respectively. Using $Co_{rich\ core}$–$Pt_{rich\ shell}$/C as the electrocatalyst of ORR, the electroactivity may be promoted by treating with acid solution to remove Co on the outer layer of the electrocatalyst.

In this study, the thermal decomposition of dicobalt octacarbinyl ($Co_2(CO)_8$) and the reduction of platinum acetylacetonate ($Pt(acac)_2$) in series were used to prepare $Co_{rich\ core}$–$Pt_{rich\ shell}$ on carbon powder (XC-72) ($Co_{rich\ core}$–$Pt_{rich\ shell}$/C). The properties and the electrochemical performances of ORR on the $Co_{rich\ core}$–$Pt_{rich\ shell}$/C electrocatalysts treated with acid aqueous solution for various times were investigated.

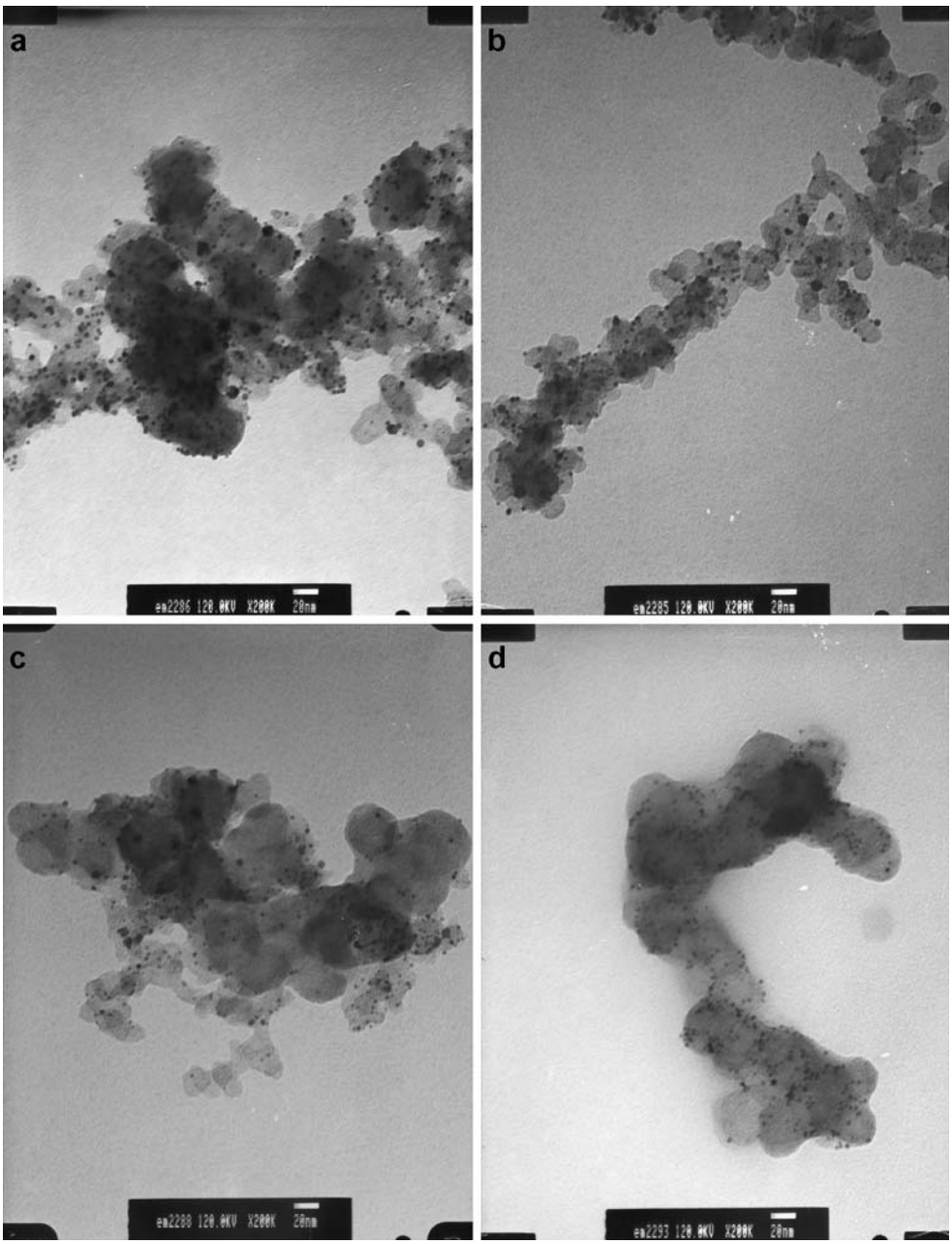

Fig. 1 TEM images of $Co_{rich\ core}$–$Pt_{rich\ shell}$/C treated with 20% $H_2SO_{4(aq)}$ for **a** 0, **b** 2, **c** 3, and **d** 4 h

Table 1 Effect of acidic treatment on the compositions of $Co_{rich\ core}$–$Pt_{rich\ shell}$/C

Acidic treatment time (h)	Co		Pt		Atomic ratio of Co/Pt
	Loading[a]	Loss of loading[b]	Loading[a]	Loss of loading[b]	
	%	%	%	%	
0	1.69	0	17.45	0	0.32
2	1.02	39.64	14.22	18.51	0.24
3	0.87	48.52	11.93	31.63	0.24
4	0.69	59.17	10.22	41.43	0.22

Atomic absorption analysis conditions: every sample was about 16–30 mg; annealed at 500 °C in air for 1 h then dissolution in 12 ml aqua regia and diluted by DI water for analyses; total volume=20 ml.

[a] Loading of Co(Pt)/%=100%×(weight of Co (Pt))/(weight of $Co_{rich\ core}$–$Pt_{rich\ shell}$).

[b] Loss of loading/%=100%×[(loading of Co (Pt))$_{t=0}$−(loading of Co (Pt))t]/(loading of Co (Pt))$_{t=0}$.

Experimental

Preparation of $Co_{rich\ core}$–$Pt_{rich\ shell}$/C

The carbon support was pretreated by mixing 5 g carbon black (XC-72, Cabot) with 50 ml 65% HNO_3 aqueous solution, heated to 100 °C for 8 h, and then filtered and washed with deionized (DI) water for several times. The obtained carbon black was dried in a vacuum oven at 70 °C for 24 h and used as the support for preparing the electrocatalyst. The solution of 60 mg $Co_2(CO)_8$ (95%, Acros) dissolved in 10 ml diphenyl ether (dpe, ≥98%, Merck) mixed with 100 mg carbon black was sparged with N_2 for 30 min, and then heated to 142 °C and refluxed in N_2 atmosphere for 30 min to prepare Co/C. Then, 50 mg platinum acetylacetonate ($Pt(acac)_2$, 98%, Strem), 100 mg 1,2-hexadecanediol (90%, Aldrich), 56 μl oleic acid (65–68%, Merck), and 61.5 μl oleylamine (70%, Aldrich) were added, and the temperature was increased to 205 °C for 1 h to reduce $Pt(acac)_2$ onto Co/C. The electrocatalyst ($Co_{rich\ core}$–$Pt_{rich\ shell}$/C) was obtained by centrifuging (6,000 rpm) and washing with ethanol two times. The pristine $Co_{rich\ core}$–$Pt_{rich\ shell}$/C was treated with 12 ml 20% H_2SO_4 for various holding times and then washing with DI water for two times, and then dried at a 100 °C vacuum oven for 24 h.

Characterization of $Co_{rich\ core}$–$Pt_{rich\ shell}$/C

The morphology of $Co_{rich\ core}$–$Pt_{rich\ shell}$/C was characterized by a transmission electron microscope (TEM, JEOL JEM-1010) with an accelerating voltage of 120 kV. The compositions of the prepared electrocatalysts, which were calcined at 500 °C for 1 h to remove carbon support and then dissolved in aqua regia, were analyzed by an atomic absorption spectrophotometer (AAS, HITACHI Z-6100). X-ray diffraction patterns of the electrocatalysts were performed in an X-ray diffractometer (SHIMADZU XRD-6000) with Cu Kα radiation (λ=1.54 Å, 40 kV, and 30 mA) over a 2θ angle from 20° to 90° at a rate of 2° min^{-1}. Because the Pt (2 2 0) peak is isolated from the diffraction peaks of the carbon black support, the mean Pt grain sizes of $Co_{rich\ core}$–$Pt_{rich\ shell}$/C were calculated based on Pt (2 2 0) according to Scherrer's formula [14]:

$$L = \frac{k\lambda}{B\cos\theta} \quad (1)$$

where L, k, and λ are the grain size of the Pt particle, a constant of 0.94, and the wavelength of the X-ray (1.54 Å), respectively. θ and B given in Eq. 1 are the diffraction angle and the half-peak broadening of Pt (2 2 0).

The working electrode of ORR was prepared by casting 35 μl electrocatalyst slurry obtained by mixing 10 mg $Co_{rich\ core}$–$Pt_{rich\ shell}$/C with 100 μl 5% Nafion® (Aldrich) and 500 μl DI water on a 1 cm^2 Au plate, and then dried in an oven at 110 °C for 30 min. The electrochemical measurement in 60 ml 0.5 M $HClO_4$ aqueous solution powered by an electrochemical analyzer (CHI 611A) was conducted in a conventional three-electrode electrochemical cell with a Pt sheet and a reversible hydrogen electrode (RHE) as the counter and reference electrodes, respectively. The electroactive areas of Pt on the electrocatalysts were measured by cyclic voltammetry (CV) with the scan range and rate of 0.05–1.2 V and 0.05 V s^{-1} in N_2 atmosphere. The electrochemical properties of ORR was studied by linear sweep voltammetry (LSV) scanned from 0.2 V to the open circuit potential (OCP) with a rate of 0.0005 V s^{-1} in the electrolyte sparged with O_2 for 30 min before the experiment. The OCP of ORR was obtained by measuring the rest potential in an open circuit status after sparging O_2 for 30 min at 25 °C.

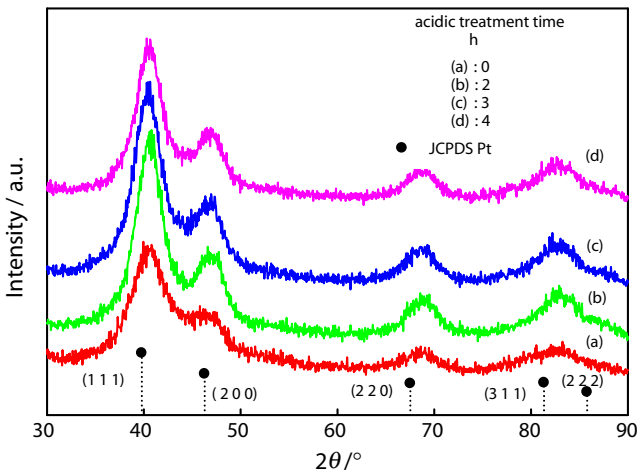

Fig. 2 XRD spectra of $Co_{rich\ core}$–$Pt_{rich\ shell}$/C treated with 20% $H_2SO_{4(aq)}$ for various times

Table 2 Effect of acidic treatment on the structure characteristics of the electrocatalysts

Acidic treatment time h	Pt (1 1 1) °	Particle size (TEM) nm	Grain size[a] (XRD) Nm	Lattice parameter nm	Degree of alloying %
0	40.76	3–8	3.17±0.008	0.3857±0.0007	16.30
2	40.64	1–6	3.19±0.003	0.3862±0.0004	14.95
3	40.57	1–6	3.22±0.019	0.3865±0.0005	14.13
4	40.32	1–6	3.26±0.015	0.3866±0.0009	13.86

[a] The grain sizes were calculated based on the crystal face of Pt (2 2 0).

Results and discussion

Particle sizes of $Co_{rich\ core}$–$Pt_{rich\ shell}$

By increasing the time of acid treatment, the dispersion of $Co_{rich\ core}$–$Pt_{rich\ shell}$ on the carbon support increased; on the other hand, the particle size of $Co_{rich\ core}$–$Pt_{rich\ shell}$ decreased as illustrated in the TEM photographs (Fig. 1). The decrease in the particle size of the $Co_{rich\ core}$–$Pt_{rich\ shell}$ on the support from 3–8 to 1–6 nm with the increase in treating time from 0 to 4 h was deduced to be the dissolution of the exposed and unprotected Co on $Co_{rich\ core}$–$Pt_{rich\ shell}$. Although the particle sizes of $Co_{rich\ core}$–$Pt_{rich\ shell}$ shown in Fig. 1b–d were found at the same range (1–6 nm) by increasing the treating time from 2 to 4 h, the fraction of the smaller particle increased with the treating time.

Compositions of $Co_{rich\ core}$–$Pt_{rich\ shell}$

The compositions of the pristine and acidic treatment $Co_{rich\ core}$–$Pt_{rich\ shell}$ on the carbon support analyzed by AAS indicated that the Co loading of $Co_{rich\ core}$–$Pt_{rich\ shell}$/C decreased from 1.69% to 1.02%, 0.87%, and 0.69% by increasing the acidic treating time from 0 to 2, 3, and 4 h, respectively (Table 1). At the same time, the Pt loadings of $Co_{rich\ core}$–$Pt_{rich\ shell}$/C decreased from 17.45% to 10.22% with the increase in the acid treatment time from 0 to 4 h. The experimental results correlated well with the results analyzed by TEM (Fig. 1) that some Co of $Co_{rich\ core}$–$Pt_{rich\ shell}$ dissolved in the acid treatment process resulted in the decrease in the particle size and the Co loading of $Co_{rich\ core}$–$Pt_{rich\ shell}$. The Co dissolution also caused the loss of less adhesive Pt from $Co_{rich\ core}$–$Pt_{rich\ shell}$/C and the decrease in the Pt loading. Increasing the acid treating time from 0 to 4 h resulted in the increase in the losing percentages of Co and Pt loadings from 0% to 59.17% and 41.43%, respectively. The decrease in the Co loading of the $Co_{rich\ core}$–$Pt_{rich\ shell}$/C was greater than that of Pt in the acid treatment process, and hence, caused the decrease in the atomic ratio of Co/Pt with the increase in the treating time. The Co/Pt atomic ratio decreased from 0.32 to 0.24 by increasing the acidic treatment time from 0 to 2 h, and the Co/Pt ratio approached a stable value of 0.22 by further increase in the treating time to 4 h (Table 1).

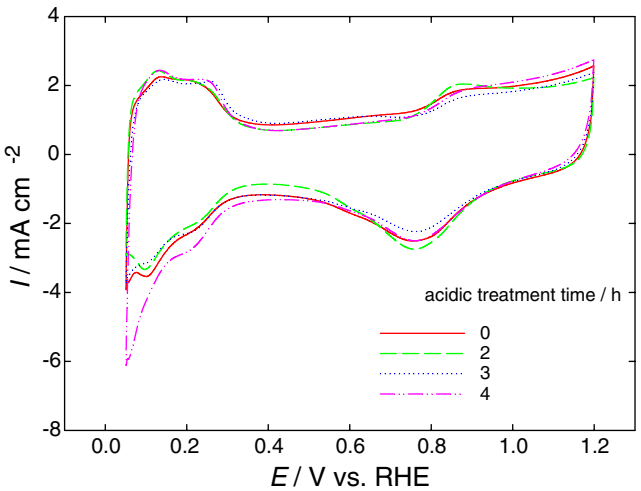

Fig. 3 Cyclic voltammograms of $Co_{rich\ core}$–$Pt_{rich\ shell}$/C treated with 20% $H_2SO_{4(aq)}$ for various times. *WE* $Co_{rich\ core}$–$Pt_{rich\ shell}$/C/Au plate with a geometric area of 1 cm^2, *RE* RHE (0.5 M $HClO_4$), *CE* Pt foil; electrolyte=0.5 M $HClO_4$, room temperature, scan rate=0.05 V s^{-1}, scan range=0.05–1.2 V

Crystallography and alloying of electrocatalysts

The Pt crystal faces of (1 1 1), (2 0 0), (2 2 0), (3 1 1), and (2 2 2) were found from the XRD spectra of $Co_{rich\ core}$–

Table 3 Effect of acidic treatment on the characteristics of ORR on $Co_{rich\ core}$–$Pt_{rich\ shell}$/C

Acidic treatment time (h)	EA[a] ($m^2\ g^{-1}$)	OCP[b] (V)	CD[c] ($mA\ cm^{-2}$)	MA[d] ($A\ g^{-1}$)	SA[e] ($\mu A\ cm^{-2}$)
0	33.22	0.9995	0.619	6.184	18.614
2	46.49	1.0025	1.054	12.912	47.716
3	47.41	1.0135	0.882	12.885	27.178
4	66.39	1.0155	0.912	15.544	23.413

The characteristics were measured at the overpotential of 0.1 V.
WE: $Co_{rich\ core}$–$Pt_{rich\ shell}$/C/Au plate with a geometric area of 1 cm^{-2}), *RE*: RHE (0.5 M $HClO_4$), *CE*: Pt foil (electrolyte=0.5 M $HClO_4$ saturated with O_2, room temperature, scan rate=0.0005 V s^{-1}, scan range=0.2–1.2 V, O_2 flow rate=40 ml min^{-1}, agitation rate=200 rpm), *EA*: electroactive area, *OCP*: open circuit potential, *CD*: current density at an overpotential of 0.1 V, *MA*: mass activity, *SA*: specific activity.

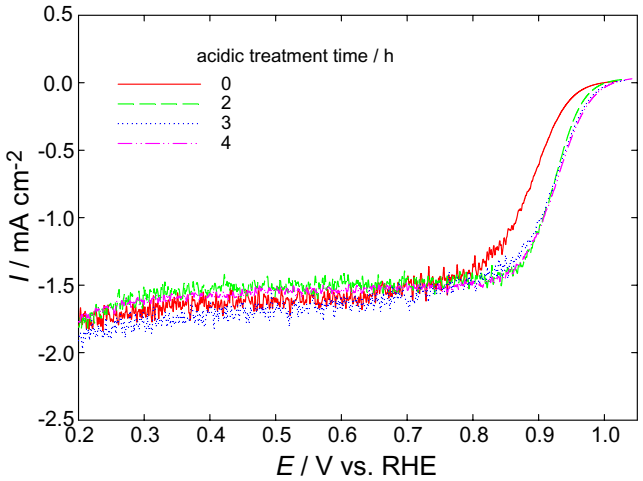

Fig. 4 Linear scan voltammograms of ORR on $Co_{rich\ core}$–$Pt_{rich\ shell}$/C/Au plate treated with 20% $H_2SO_{4(aq)}$ for various times. *WE* $Co_{rich\ core}$–$Pt_{rich\ shell}$/C/Au plate with a geometric area of 1 cm^{-2}, *RE* RHE (0.5 M $HClO_4$), *CE* Pt foil; electrolyte=0.5 M $HClO_4$ saturated with O_2, room temperature, scan rate=0.0005 V s^{-1}, scan range=0.2–1.2 V, O_2 flow rate=40 ml min^{-1}, agitation rate=200 rpm

$Pt_{rich\ shell}$/C as indicated in Fig. 2. The Pt grain sizes calculated based on Pt (2 2 0) by using Scherrer's equation [14] were obtained to be 3.18, 3.19, 3.22, and 3.26 nm, respectively, for the acidic treating time of 0, 2, 3, and 4 h (Table 2). The increase in Pt grain size analyzed by XRD with the acidic treating time was deduced to be the loss of the small grain size of Pt in the acidic treatment process, which was demonstrated by the fact that the Pt loading decreased with the acidic treating time (Table 1). Furthermore, due to the dissolution of Co near the surface of the $Co_{rich\ core}$–$Pt_{rich\ shell}$ particle, which was rich in Pt, in the acidic treating process caused the decrease in the intercalation of Co into the Pt crystal structure and the increase in Pt lattice parameter as illustrated in Table 2. The lattice parameter of Pt increased from 0.3857 to 0.3866 nm when the time for $Co_{rich\ core}$–$Pt_{rich\ shell}$/C treated with 20% H_2SO_4 aqueous solution increased from 0 to 4 h (Table 2). Based on the results in the shift of diffraction angle and the change in the Pt lattice parameter, the alloying degree of the $Co_{rich\ core}$–$Pt_{rich\ shell}$ treated with acid solution for 0, 2, 3, and 4 h were calculated according to Vegard's law [15] to be 16.30%, 14.95%, 14.13%, and 13.86%, respectively (Table 2). The segregation of the Co core and Pt shell phases hence increased with the acidic treatment time.

Electroactive area of electrocatalysts

Using $Co_{rich\ core}$–$Pt_{rich\ shell}$/C treated with 20% H_2SO_4 aqueous solution for various times as the cathodic electrocatalysts, the cyclic voltammograms in 0.5 M $HClO_4$ aqueous solution sparged with N_2 for 30 min to remove dissolving O_2 were illustrated in Fig. 3. The Pt electroactive area can be determined from the desorption charge of the hydrogen atoms adsorbed on the electrode. This desorption charge is attributed to one hydrogen atom per Pt electroactive site (Pt_s–H→Pt_s+H^++e^-), which amounts approximately to 210 μC cm^{-2} after double layer charge subtraction for a polycrystalline surface [16]. The electroactive area of $Co_{rich\ core}$–$Pt_{rich\ shell}$/C significantly increased from 33.22 to 66.39 m^2 g^{-1} by increasing the acidic treating time from 0 to 4 h (Table 3). The results indicated that the dissolution of Co in the acidic treatment procedure caused the increase in the surface roughness and the Pt electroactive area of the electrocatalysts.

ORR on electrocatalysts

The OCP of the pristine $Co_{rich\ core}$–$Pt_{rich\ shell}$/C was obtained to be 0.9995 V in the 0.5 M $HClO_4$ aqueous solution sparged with 40 ml min^{-1} O_2 for 30 min, and the OCP increased to 1.0155 V for the electrocatalyst treated with 20% H_2SO_4 for 4 h as illustrated in Fig. 4 and Table 3. Compared with the pristine electrocatalyst, the LSVs of ORR on $Co_{rich\ core}$–$Pt_{rich\ shell}$/C treated with acid solution was shifted to the positive potential direction. Furthermore, the overpotential of ORR on the electrocatalysts treated with acid solution for a fixed current density (CD) was less than that of pristine $Co_{rich\ core}$–$Pt_{rich\ shell}$/C (Fig. 4). The experimental results indicated that the kinetics of ORR on $Co_{rich\ core}$–$Pt_{rich\ shell}$/C treated with acid solution was greater than that on the pristine electrocatalyst.

Using the commercial Pt electrocatalyst (20% Pt/C, E-TEK) as the cathode, the shift of LSVs of ORR in 0.5 M $HClO_4$ aqueous solution to the direction of negative

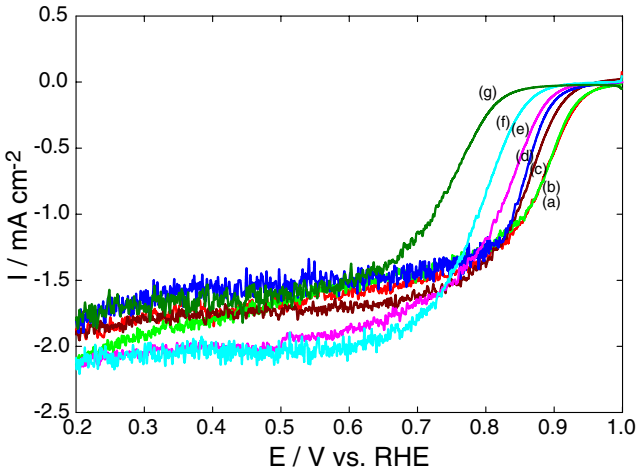

Fig. 5 Linear scan voltammograms of ORR on 20% Pt/C (E-TEK)/Au plate in 0.5 M $HClO_{4(aq)}$ in the presence of *a* 0, *b* 10^{-8}, *c* 10^{-7}, *d* 10^{-6}, *e* 10^{-5}, *f* 10^{-4}, and *g* 10^{-3} M Co^{2+}. *WE* 20% Pt/C (E-TEK)/Au plate with a geometric area of 1 cm^2, *RE* RHE (0.5 M $HClO_4$), *CE* Pt foil; electrolyte=0.5 M $HClO_4$ saturated with O_2, room temperature, scan rate=0.0005 V s^{-1}, scan range=0.2–1.2 V, O_2 flow rate=40 ml min^{-1}, agitation rate=200 rpm

potential increased with the increase in the concentration of Co^{2+} in the solution (Fig. 5). Meanwhile, the OCP of ORR decreased and the overpotential for a fixed CD increased by increasing the concentration of Co^{2+} in the electrolyte. These results revealed that the kinetics of ORR on the Pt electrocatalyst would be retarded by the presence of Co^{2+} in the electrolyte. Similar results were also reported in the literature [12, 17–19]. The trace levels of copper ion might present in the real ORR system, mostly as a corrosion product, and had been proved to have devastating inhibiting effect on the ORR [17–19]. The inhibition of the kinetics of ORR is deduced to be the adsorption of the transition metal ions on the Pt active site to slow down the reaction of oxygen reduction [12, 17–19].

When the $Co_{rich\ core}$–$Pt_{rich\ shell}$/C electrocatalysts were treated with acid solution and used as the cathodes of ORR, the dissolution of Co from the electrocatalyst into the electrolyte would be significantly decreased. Therefore, compared with the pristine electrocatalyst, the kinetics of ORR on the electrocatalyst treated with the acid solution was significantly increased as illustrated in Fig. 4. For the overpotential of 0.1 V, the CD of ORR on $Co_{rich\ core}$–$Pt_{rich\ shell}$/C treated with 20% H_2SO_4 aqueous solution for 0, 2, 3, and 4 h were obtained to be 0.619, 1.054, 0.882, and 0.912 mA cm^{-2}, respectively (Table 3). Accordingly, the MAs and SAs of the $Co_{rich\ core}$–$Pt_{rich\ shell}$/C treated with acid for various times were significantly greater than that of the pristine $Co_{rich\ core}$–$Pt_{rich\ shell}$/C (Table 3). The acidic treatment electrocatalysts exhibited higher ORR activities due to the higher surface area and less inhibitor (Co^{2+}) dissolved from $Co_{rich\ core}$–$Pt_{rich\ shell}$/C into the electrolyte for studying ORR. However, in general, the less lattice parameter and higher alloying degree of Pt–M were favored to the activities of ORR [3]. Hence, the maximum SA was obtained to be 47.716 μA cm^{-2} on $Co_{rich\ core}$–$Pt_{rich\ shell}$/C treated with 20% H_2SO_4 aqueous solution for 2 h. The maximum electroactive area of Pt obtained for $Co_{rich\ core}$–$Pt_{rich\ shell}$/C treated with acidic solution for 4 h resulted in a maximum MA of ORR (15.544 A g^{-1}) due to its maximum electroactive area of 66.39 m^2 g^{-1} (Table 3).

Conclusions

The characteristics of $Co_{rich\ core}$–$Pt_{rich\ shell}$/C prepared by thermal decomposition, chemical reduction, and modification with acidic treatment were investigated. Due to the Co dissolution and the loss of the less adhesive Pt from the prepared electrocatalysts, the Co and Pt loadings decreased from 17.45% and 1.69% to 10.22% and 0.69%, respectively, by increasing the acidic treating time from 0 to 4 h. Increasing the acidic treating time resulted in the increase in the Pt electroactive area and the decrease in the dissolution of Co from the electrocatalysts into the electrolyte, then the kinetics of ORR was enhanced. On the other hand, the increase in the Pt lattice parameter from 0.3857 to 0.3866 nm and the decrease in the alloying degree of $Co_{rich\ core}$–$Pt_{rich\ shell}$ from 16.30% to 13.86% for increasing the acidic treatment time from 0 to 4 h caused the decrease in the kinetics of ORR. Therefore, the maximum CD of ORR with the overpotential of 0.1 V was obtained to be 1.054 μA cm^{-2} when the electrocatalyst was treated with acid solution for 2 h. Further increase in the acidic treating time decreased the CD. The maximum MA and SA of ORR were obtained to be 15.544 A g^{-1} and 47.716 μA cm^{-2} when the $Co_{rich\ core}$–$Pt_{rich\ shell}$/C was treated with acid solution for 4 and 2 h, respectively.

Acknowledgment The financial support of the National Science Council Republic of China (Project number: NSC 95-2120-M-011-002) and Tunghai University is acknowledged.

References

1. Carrette L, Friedrich KA, Stimming U (2001) Fuel Cells 1:5
2. Alonso-Vante N, Tributsch H (1986) Nature 323:431
3. Markovic NM, Schmidt TJ, Stamenkocic V, Ross PN (2001) Fuel Cells 2:105
4. Shim J, Yoo DY, Lee JS (2000) Electrochim Acta 45:1943
5. Wakabayashi N, Takeichi M, Uchida H, Watanabe M (2005) J Phys Chem B 109:5836
6. Yu P, Pemberton M, Plasse P (2005) J Power Sources 144:11
7. Landsman DA, Luczak FJ (2003) In: Vielstich W, Lamm A, Gasteiger HA (eds) Handbook of fuel cells: fundamentals, technology, and applications. vol. 4. Wiley, New York Chapter 65
8. Okada T (2003) In: Vielstich W, Lamm A, Gasteiger HA (eds) Handbook of fuel cells: fundamentals, technology, and applications. vol. 3. Wiley, New York Chapter 37
9. Okada T, Ayato Y, Yuasa M, Sekine I (1999) J Phys Chem B 103:3315
10. Okada T, Ayato Y, Satou H, Yuasa M, Sekine I (2001) J Phys Chem B 105:6980
11. Adžić RR, Wang JX (2000) Electrochim Acta 45:4203
12. Toda T, Igarashi H, Uchida H, Watanabe M (1999) J Electrochem Soc 146:3750
13. Do JS, Chen YT, Lee MH (2007) J Power Sources 172:623
14. West AR (1984) Solid state chemistry and its applications. Wiley, New York
15. Katayama AA, Nakajima H, Fujikama K, Kita H (1983) Electrochim Acta 28:777
16. Marković NM, Gasteiger HA, Grgur BN, Ross PN (1999) J Electroanal Chem 467:157
17. Stamenkvić V, Marković NM (2001) Langmuir 17:2388
18. Wei Z, Guo H, Tang Z (1996) J Power Sources 62:233
19. Colon-Mercado HR, Kim H, Popov BN (2004) Electrochem Commun 6:795